Finite Element Analysis of MEMS Diaphragm Valves

Fuqian Yang and Imin Kao
Systems Engineering and Integration Laboratory
Department of Mechanical Engineering
SUNY at Stony Brook, Stony Brook, NY 11794-2300
Email:yang@mal.eng.sunysb.edu

Abstract

Based on simple plate theory, the deflection of MEMS microvalve is studied analytically and numerically. The critical load to initially drive the microvalve is found to be proportional to the pre-deflection of microdiaphragm. The microdiaphragm becomes stiffer when either central pedestal or the diaphragm thickness increases. These decrease the deformation ability of the microdiaphragm, which in turn reduce the possibility of in-use stiction. The finite element results show that stress concentration around the corner of the central pedestal and the step occurs, which may result in local mechanical failure and influence the lifetime of the microsystems.

Keywords: MEMS valve, plate theory, critical load, finite element analysis

INTRODUCTION

A number of microvalves suitable for fluid flow modulating have been reported in literature. The mechanisms include electrostatic actuation [1], [2], bimetallic-differential thermal expansion [3], piezoelectric [4], magnetic [1], [5], thermopneumatic [6], and shape memory effects [7], [8]. One of the recent design of diaphragm microvalves is fluid-driven and pressure-balanced [9], [10], which use fluids (such as air) generating pressure difference across the diaphragm to provide a driving force for the actuator. The function of these microvalves depends on the stiffness of a silicon diaphragm; therefore, the valves have strokes of only a few tens of microns [8]. At these levels of stroke, the required energy to modulate the fluid flow are much higher than that most mechanisms can generate. Of the above mentioned mechanisms, only the fluid-driven, thermopneumatic, and shape memory actuation have sufficiently high actuation energy for liquid flow modulations. The distinct advantage of the fluid-driven mechanism is the reduction of power consumption, compared to the thermally actuated valves such as the IC sensors valve or HP valve.

Huff *et al.* [10], using laminar flow theory and simple plate theory, studied the deflection of microvalves in the fluid-driven and pressure-balanced microvalves.

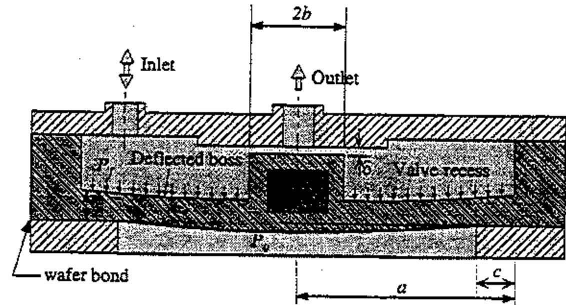

Figure 1: schematic diagram of pressure-balanced MEMS microvalves

However, they did not address the interaction between fluid and the microdiaphragm. Based on the inviscid fluid flow and simple plate theory, Yang and Kao [11] analyzed the effect of the fluid-valve interaction on the function of the microvalve systems. They found a unstable working zone within which the microsystems may fail. However, there is few study on microvalves from the viewpoint of system design. To optimize the design of microvalves, which is subjected to dynamic loading, it is the purpose of this work, using simple plate theory together with finite element analysis, to investigate the mechanical behavior of the fluid-driven microvalves and provide a basis for MEMS valve design.

DEFORMATION OF MICROVALVE

Figure 1 shows the schematic diagram of pressure balanced microvalves. Fluid flows into the microchamber at inlet and exits at outlet. This generates a pressure difference across the diaphragm and provides a driving force to monitor the deformation of the valve. Under small deformation, the simple plate theory is used. The governing equation of the MEMS microvalve deflection is

$$\nabla^4 w = \frac{\Delta P}{D} \tag{1}$$

where w is the diaphragm transverse deflection, ΔP $(= P_f - P_0)$ is the pressure difference across the microdiaphragm, P_f is the hydrostatic pressure in the fluid, P_0 is the constant pressure applied to the valve on the

other side, and $D=Ed^3/12(1-\nu^2)$ is the bending stiffness, E is Young's modulus, ν is the Poisson ratio, and d is the thickness of the microvalve. For the microvalve shown in Figure 1, the boundary conditions at the outer edge are

$$w = \frac{dw}{dr} = 0 \qquad \text{at } r = a \tag{2}$$

Critical load to open MEMS valve

As shown in Figure 1, the microdiaphragm is pre-deformed to seal fluid flow. To open the seal and push fluid to flow through the microchamber between the diaphragm and the substrate, an initial constant pressure difference has to be applied onto the surface of the diaphragm to drive the diaphragm. For simplicity, the central pedestal at the center of the diaphragm is assumed rigid and the effect of c at the out edge is neglected (whose effect will be analyzed in the finite element calculation). The boundary conditions at the inner edge are

$$w = \delta \text{ and } \frac{dw}{dr} = 0 \qquad \text{at } r = b \tag{3}$$

where δ is the pre-deflection of the MEMS microvalve. For the constant pressure difference ΔP, the general solution of equation (1) is

$$w = \frac{\Delta P}{64D} r^4 + C_1 \frac{r^2}{4} + C_2 \ln \frac{r}{a} + C_3 \tag{4}$$

Using the boundary conditions (2 and 3), the diaphragm deflection is

$$w = \frac{\Delta P}{64D}\left(r^4 + a^4 + 2a^2b^2 - 2r^2(a^2+b^2) + 4a^2b^2 \ln \frac{r}{a}\right) \tag{5}$$

which gives the critical pressure difference (ΔP_c) to initiate the operation of the microvalve as

$$\frac{\Delta P_c}{\delta} = \frac{64D}{a^4 - b^4 + 4a^2b^2 \ln \frac{b}{a}} \tag{6}$$

Figure 2 shows the dependence of ΔP_c on the central pedestal size and the pre-deflection of the microdiaphragm.

For small deformation, the critical pressure difference is proportional to the pre-deflection of the microdiaphragm as shown in equation (6) and it increases nonlinearly with increasing pedestal size. For large deformation and non-pedestal MEMS microvalve structure, the first order solution of the microdiaphragm deflection is [12]

$$w = \delta(1 - r^2/a^2)^2 \tag{7}$$

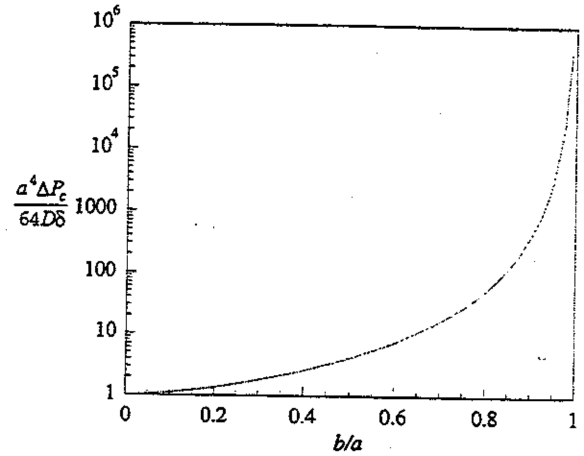

Figure 2: Effect of the pedestal size on the critical pressure difference

and

$$\frac{a^4 \Delta P_c}{64D\delta} = 1 + 0.488\frac{\delta^2}{d^2} \tag{8}$$

which is a third-order relationship between the critical load and the pre-deflection of the microdiaphragm.

Stiffness of the microdiaphragm

One of the important parameters in the mechanical design of microvalves is the stiffness of the microdiaphragm, which controls the deformation capability of the microdiaphragm. Considering a symmetrical ring load (with q as the line load density) applied onto the diaphragm surface, the pressure difference across the microdiaphragm becomes

$$\Delta P = q\delta(r - r_0) \tag{9}$$

and assuming the central pedestal to be rigid, the boundary condition at the inner edge is

$$\frac{dw}{dr} = 0 \qquad \text{at } r = b \tag{10}$$

The transverse deflection of the microdiaphragm is,

for $b \leq r \leq r_0$

$$w = \frac{a^2 r_0 q}{4D}\frac{a^2}{a^2-b^2}\left\{\left(1-\frac{r_0^2}{a^2}\right)\left[\left(1-\frac{b^2}{a^2}\right) - \frac{1}{2}\left(1-\frac{r^2}{a^2}\right)\right] + \frac{b^2}{a^2}\left(1-\frac{r_0^2}{a^2}\right)\ln\frac{r_0}{r} + \left(2\frac{b^2}{a^2} - \frac{r_0^2}{a^2} - \frac{r^2}{a^2}\right)\ln\frac{a}{r_0} - \frac{2b^2}{a^2}\ln\frac{a}{r}\ln\frac{a}{r_0}\right\} \tag{11}$$

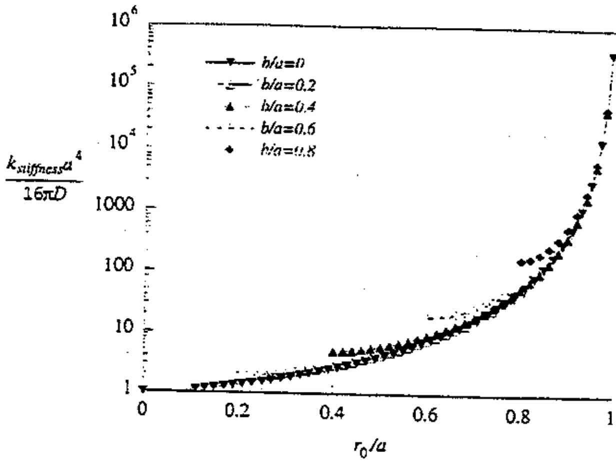

Figure 3: Stiffness of the microdiaphragm under a ring load

and for $r_0 \le r \le a$

$$\begin{aligned} w &= \frac{a^2 r_0 q}{4D}\frac{a^2}{a^2-b^2}\left\{\left(1-\frac{r^2}{a^2}\right)\left[\left(1-\frac{b^2}{a^2}\right)\right.\right.\\ &\left.-\frac{1}{2}\left(1-\frac{r_0^2}{a^2}\right)\right]+\frac{b^2}{a^2}\left(1-\frac{r^2}{a^2}\right)\ln\frac{r}{r_0}\\ &\left.+\left(2\frac{b^2}{a^2}-\frac{r_0^2}{a^2}-\frac{r^2}{a^2}\right)\ln\frac{a}{r}-\frac{2b^2}{a^2}\ln\frac{a}{r}\ln\frac{a}{r_0}\right\} \end{aligned} \quad (12)$$

Let $r = r_0$ and $F = 2\pi r_0 q$ (the total load), both equations (11) and (12) give the stiffness ($k_{stiffness}$) of the microdiaphragm as follows

$$k_{stiffness} = \frac{dF}{dw} = \frac{16\pi D(a^2-b^2)}{f} \quad (13)$$

$$\begin{aligned} f = {} & a^4 - 2a^2b^2 + 2b^2r_0^2 - r_0^4 + 4a^2(b^2-r_0^2)\\ & \ln(a/r_0) - 4a^2b^2\ln^2(a/r_0) \end{aligned} \quad (14)$$

Figure 3 shows the stiffness change of the diaphragm. The stiffness increases as the loading approaches the outer edge in which the pedestal has little influence. It also increases with increasing the pedestal size. This provides us a method to change the compliance of the microdiaphragm.

When the ring load is applied onto the central pedestal, equation (12) gives the diaphragm deflection

$$\begin{aligned} w &= \frac{a^2 F}{8\pi D}\frac{a^2}{a^2-b^2}\left\{\frac{1}{2}\left(1-\frac{r^2}{a^2}\right)\left(1-\frac{b^2}{a^2}\right)\right.\\ &+\frac{b^2}{a^2}\left(1-\frac{r^2}{a^2}\right)\ln\frac{r}{b}\\ &\left.+\left(\frac{b^2}{a^2}-\frac{r^2}{a^2}\right)\ln\frac{a}{r}-\frac{2b^2}{a^2}\ln\frac{a}{r}\ln\frac{a}{b}\right\} \end{aligned} \quad (15)$$

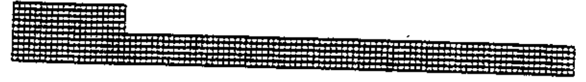

Figure 4: Finite element mesh of the diaphragm

and the stiffness is

$$k_{stiffness} = \frac{16\pi D(a^2-b^2)}{(a^2-b^2)^2 - 4a^2b^2\ln^2(a/b)} \quad (16)$$

FINITE ELEMENT COMPUTATION

Finite element mesh

To analyze the effect of central pedestal size on the microdiaphragm deflection, finite element was used here for two different cases, case I:

$$\Delta P = 0 \qquad \text{for } 0 < r < b \quad (17)$$

and case II

$$\Delta P|_{0\le r\le b} = \Delta P|_{b<r\le a} \quad (18)$$

For the case I, the hydrostatic pressure is applied only in the region of $b < r < a$, and for case II, the pressure is applied over the diaphragm surface $0 < r < a$. A typical mesh of a clamped circular diaphragm with radius of 1 mm is shown in Figure 4, in which four-node quadrilateral solid element was employed. To simulate the deflection process, a uniform pressure is imposed on the diaphragm surface. This deforms the diaphragm and gives the corresponding deflection. Our simulation used the large deformation feature of the ABAQUS finite element package [13]. In the following calculation, we assume that the microdiaphragm is made of silicon and use the parameters, E = 169 GPa and μ = 0.358 along the (111) direction for single crystalline silicon [14].

To test the model, a point load was applied at the center of the diaphragm. As shown in Figure 5, the relation between the displacement of the diaphragm (w_0) at the center and the applied load (F) was compared with the analytical results for small deformation [12]

$$w_0 = \frac{3Fa^2(1-\nu^2)}{4\pi E d^3} \quad (19)$$

and the first order solution for large deformation [12]

$$w_0 = \frac{3Fa^2(1-\nu^2)}{4\pi E d^3} - \frac{573}{2592}\cdot\frac{(1-\nu^2)w_0^3}{d^2} \quad (20)$$

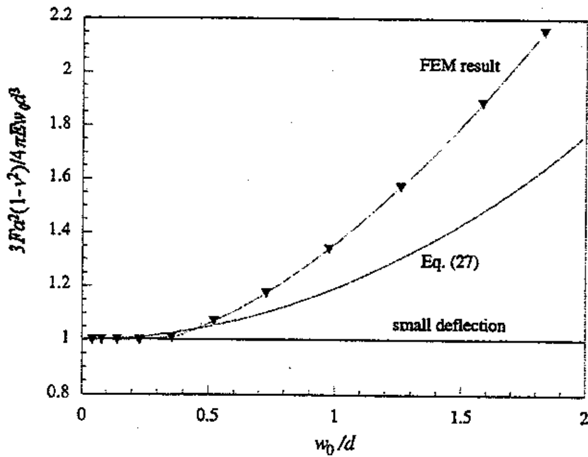

Figure 5: Center displacement under a concentrated load

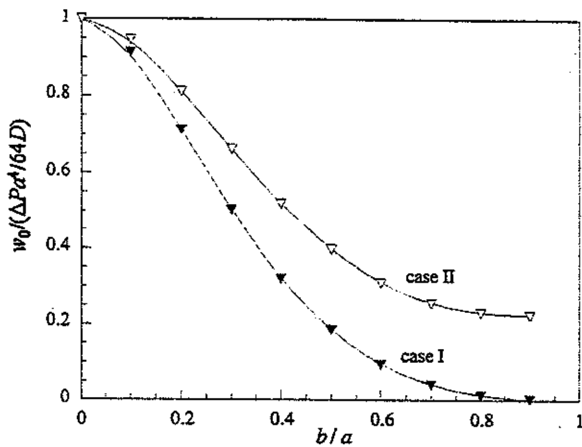

Figure 6: Effect of the pedestal size on the diaphragm deflection ($d/a = 0.05$, $h/d = 1$, and $c = 0$)

It is seen that, the FEM results are in agreement with equation (19) for small deformation up to about $w_0/d = 0.35$. Beyond that, it deviates from the expression due to large deformation. Equation (19) has been confirmed experimentally within the elastic range for small deformation [15]. The FEM results are approximately in agreement with equation (20) of the first order solution for deflection up to $w_0/d = 0.5$.

Effect of pedestal size

To analyze the effect of the pedestal size on the relation between the load and the diaphragm deflection, several different pedestal radii were used. Figure 6 shows that diaphragm deflection under the deformation condition decreases with increasing pedestal size for both case I and case II. This is due to the increase of the diaphragm bending stiffness by increasing the pedestal size. This indicates that the critical load to initially drive the diaphragm increases with pedestal size and more energy is required to operate the microvalve systems. The difference between case I and case II obviously is due to the different loading conditions.

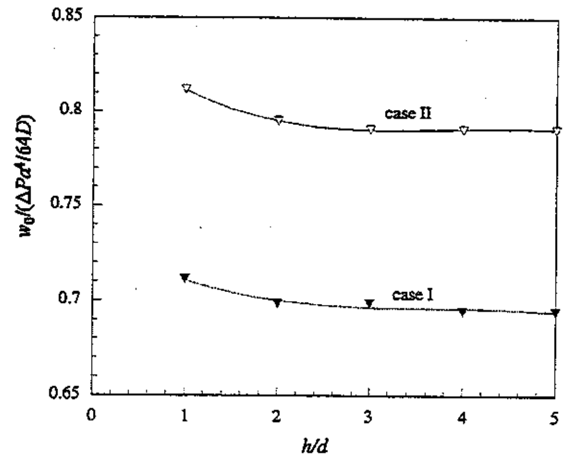

Figure 7: Dependence of diaphragm deflection on pedestal thickness ($d/a = 0.05$, $b/a = 0.1$, and $c = 0$)

Dependence of the diaphragm deflection on the pedestal thickness (h) under small deformation condition is plotted in Figure 7. The diaphragm deflection decreases with increasing pedestal thickness to $h/d = 3$, which actually increases the stiffness of the microvalve. Further increase in the pedestal thickness does not change the diaphragm deflection magnitude - the pedestal can be treated as rigid. This provides us a condition for the design of the pedestal thickness, about three times larger than the diaphragm thickness is required if we want to ignore the effect of pedestal deformation on the diaphragm deflection.

Effect of diaphragm thickness

One of the important parameters in the MEMS microvalve design is the diaphragm thickness. For small deformation, the diaphragm deflection as shown in Figure 8 for both cases decreases with increasing diaphragm thickness. Under the calculation conditions, $h/a = 0.05$, $b/a = 0.1$, and $c = 0$ and small deformation, the diaphragm deflection drops about one order of magnitude when the valve thickness doubles. The increase or decrease of the diaphragm thickness dramatically change the diaphragm bending stiffness, which is proportional to the cube of the diaphragm thickness. Thicker diaphragms will require more energy input to operate; while thinner ones may easily lead to the failure of the systems, such as stiction and fracture. A compromise between energy input and the lifetime of the microsystem has to be reached for the design and fabrication of the MEMS microvalves.

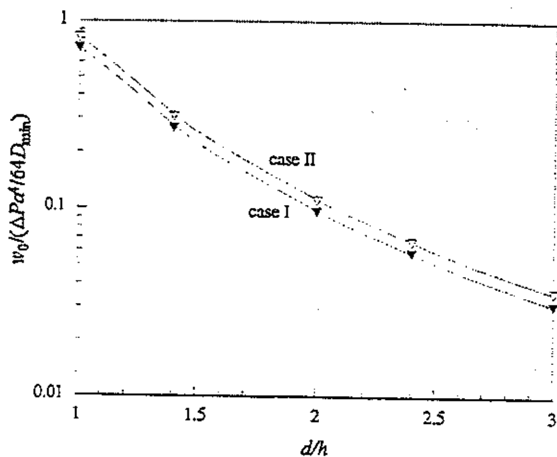

Figure 8: Dependence of the diaphragm deflection on the diaphragm thickness ($h/a = 0.05$, $b/a = 0.1$, and $c = 0$)

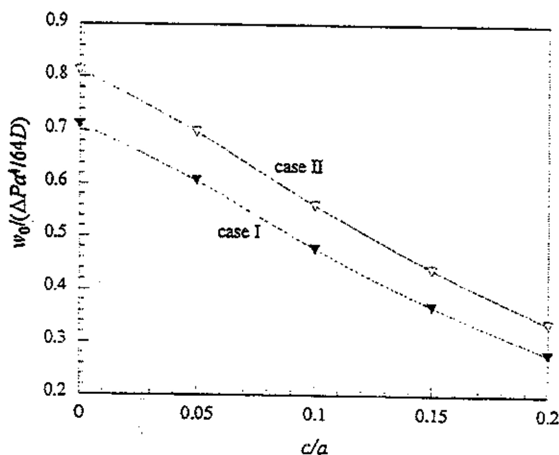

Figure 9: Effect of the edge size on the diaphragm deflection ($h/a = 0.05$, $b/a = 0.1$, and $d/a = 0.05$)

Effect of the edge size

In the actual design and fabrication of the MEMS microvalves, there is always a step at the outer edge as shown in Figure 1 to support the diaphragm. The size and deformability of the step will influence the deflection magnitude of the diaphragm and the function of the microsystems. For simplicity, we assume the step is rigid comparing to the silicon wafer and ignore the step deformation in the following analysis.

For small deformation, the diaphragm deflection as shown in Figure 9 for both cases decreases with increasing the step size. It starts with 0.81 for case II and 0.71 for case I without the step and decreases to 0.56 for case II and 0.48 for case I at c/a=0.1. Figure 10 shows the deformation of the microidiaphragm for case II under the condition $h/a = 0.05$, $b/a = 0.1$, $d/a = 0.05$, $c/a = 0.1$, $a = 1$ mm, and a pressure difference of 30 Pa. There is

Figure 10: Deflection of the microdiaphragm under case II loading condition

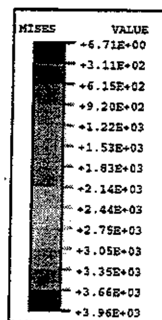

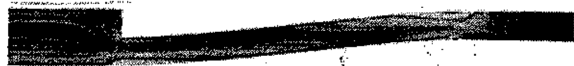

Figure 11: von-Mises stress distribution inside the microdiaphragm under case II loading condition

little deflection for the layer of material above the step. The step works as a constraint applied onto the microdiaphragm to control its mobility. This will increase power consumption to operate the microsystem and the stress concentration around the corner as shown in the following stress analyses. However, it may reduce the possibility of in-use stiction problem because a larger force is required to keep the valve to adhere to the substrate.

The von-Mises stress distribution inside the diaphragm for case II under the above conditions is shown in Figure 11. Stress concentration occurs at four different locations. The highest von-Mises stress is around the edge of the step, in which the valve may fail mechanically first. The minimum and maximum principal stresses developed inside the diaphragm can also be found. The downward diaphragm deflection creates maximum compressive stress at the edge of the step and the corner of the pedestal. On the other side, maximum tensile stress occurs on the surface of the diaphragm above the edge of the step and underneath the corner of pedestal. Cracks can be initiated at the locations of the stress concentration. This may lead to the mechanical failure of the microsystem. In addition, under the dynamic loading condition, the stress status changes from compression to tension alternatively on the surface of the diaphragm. This may result in mechanical fatigue which can be attributed to one of the failure mechanisms of the microsystems.

CONCLUSION

Using simple plate theory, the deflection of the MEMS microdiaphragm is studied analytically and numerically. The bending stiffness of the microdiaphragm increases with increasing pedestal size. Larger bending stiffness increases the corresponding energy required to initially drive the valve and the energy consumption to operate the microsystem. However, this reduces the possibility of in-use stiction failure. Using the finite element package ABAQUS, we found that the effect of pedestal deformation on the diaphragm deflection can be neglected when its thickness is over three time larger than the pedestal thickness. Stress concentration around the corner of the pedestal and the step was found, in which plastic deformation and crack can be initiated and propagated. This may result in local mechanical failure and influence the lifetime of the microsystems. The results provide us a basis to optimally design MEMS diaphragm valves.

REFERENCES

[1] D. Bosch, B. Heimhofer, G. Muck, H. Seidel, U. Thumser, and W. Welser. A silicon microvalve with combined electromagnetic/electrostatic actuation. *Sensors and Actuators*, A37-38:684, 1993.

[2] T. Ohnstein, T. Fukiura, J. Ridley, and U. Boone. Micromachined silicon microvalve. In *Proc. IEEE Micro Electro Mechanical Systems*, page 95, Napa Valley , CA, 1990.

[3] P. L. Bergstrom, J. Ji, Y. N. Liu, M. Kaviany, and K. D. Wise. Thermally driven phase-change microactuation. *J. Microelectromechanical Syms*, 4:10–17, 1995.

[4] H. T. G. van Lintel, F. C. M. van de Pol, and A. Brouwstra. A piezoelectric micropump based on micromachining of silicon. *Sensors and Actuators*, 15:163, 1988.

[5] R. L. Smith, R. W. Bower, and S. D. Collins. The design and fabrication of a magnetically actuated micromachined flow valve. *Sensors and Actuators*, A24:47, 1990.

[6] M. J. Zdeblick, R. Anderson, J. Jankowski, B. Kline-Schoder, L. Christel, R. Miles, and W. Weber. Thermopneumatically actuated microvalves and integrated electroc-fluidic circuits. In *Proc. IEEE Solid State Sensors and Actuators Workshop*, page 251, 1994.

[7] C. A. Ray, C. L. Sloan, A. D. Johnson, J. D. Busch, and R. B. Petty. A silicon-based shape memory alloy microvalve. *Mat. Res. Soc. Symp. Proc.*, 276:161, 1992.

[8] H. Kahn, W. L. Benard, M. A. Huff, and A. H. Heuer. Titanium-nickel shape memory thin film actuators for micromachined valves. *Mat. Res. Soc. Symp. Proc.*, 444:227, 1997.

[9] M. A. Huff and M. A. Schmidt. Fabrication packaging and testing of a wafer-bonded microwafer. In *Proc. IEEE Solid State Sensor and Actuator Workshop*, pages 194–197, Hilton Head Island, SC, June 1992.

[10] M. A. Huff, M. S. Mettner, T. A. Lober, and M. A. Schmidt. A pressure-balanced electrically-actuated microvalve. In *Proc. IEEE Solid State Sensor and Actuator Workshop*, pages 123–127, Hilton Head Island, SC, June 1990.

[11] F. Yang and I. Kao. Analysis of flow and stress for pressure balanced mems diaphragm valves. *in Preparation*, 1998.

[12] S.P. Timoshenko. *Theory of Plates and Shells.* McGraw-Hill, New York, 1940.

[13] ABAQUS. *ABAQUS/Standard.* HIBBITT, KARLSSON & SORENSEN, INC., New York, 5.5 edition, 1995.

[14] J. J. Wortman and R. A. Evans. Young's modulus, shear modulus and poisson's ratio in silicon and germanium. *J. Appl. Phys.*, 36:153–156, 1965.

[15] A. P. Boresi, R. J. Schmidt, and O. M. Sidebottom. *Advanced Mechanics of Materials.* John Wiely & Sons, Inc., New York, 5 edition, 1993.